Journal Pre-proof

Theta-encoded information flow from dorsal CA1 to prelimbic cortex drives memory reconsolidation

Andressa Radiske, María Carolina Gonzalez, Janine I. Rossato, Sergio Conde-Ocazionez, Martín Cammarota

PII: S2589-0042(25)01082-X

DOI: https://doi.org/10.1016/j.isci.2025.112821

Reference: ISCI 112821

To appear in: *ISCIENCE*

Received Date: 22 November 2024

Revised Date: 12 April 2025

Accepted Date: 15 May 2025

Please cite this article as: Radiske, A., Gonzalez, M.C., Rossato, J.I., Conde-Ocazionez, S., Cammarota, M., Theta-encoded information flow from dorsal CA1 to prelimbic cortex drives memory reconsolidation, *ISCIENCE* (2025), doi: https://doi.org/10.1016/j.isci.2025.112821.

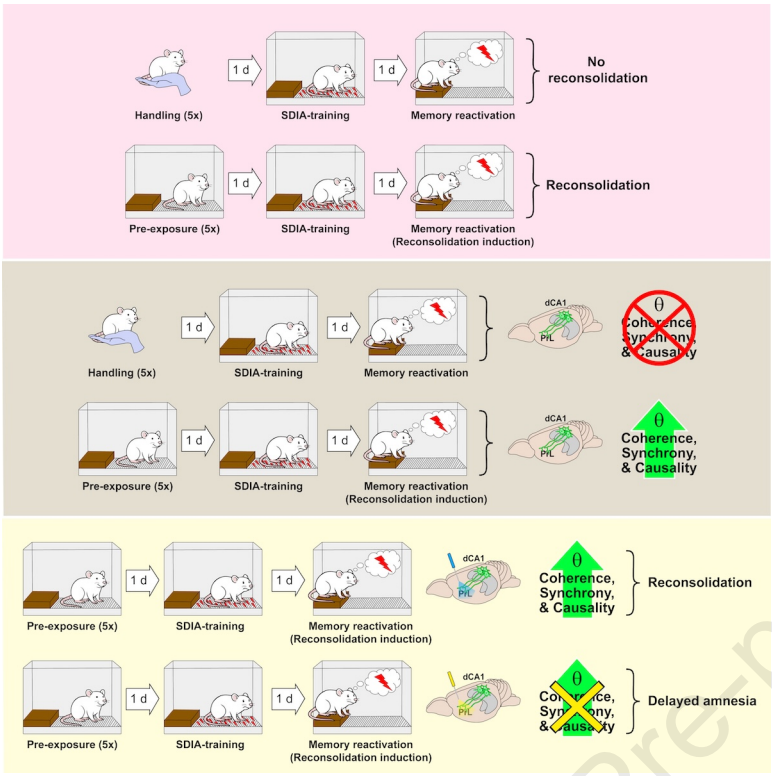

Theta-encoded information flow from dorsal CA1 to prelimbic cortex drives memory reconsolidation

Andressa Radiske[1,2], María Carolina Gonzalez[1,2], Janine I. Rossato[1], Sergio Conde-Ocazionez[1], and Martín Cammarota[1,3,4,*]

[1]Memory Research Laboratory - Brain Institute, UFRN, Natal, RN, Brazil
[2]Edmond and Lily Safra International Institute of Neuroscience, Macaiba, RN, Brazil
[3]Senior author
[4]Lead contact
*Correspondence: martin.cammarota@neuro.ufrn.br

SUMMARY

Reconsolidation is the process by which reactivated, labile memories are restabilized. Disrupting this process induces retrograde amnesia specific to the reactivated memory, making it a promising therapeutic target for anxiety disorders rooted in maladaptive avoidance. However, the electrophysiological mechanisms underlying reconsolidation are still not fully understood, limiting its translational potential. Here, we show that inducing reconsolidation of a fear-driven avoidance memory in adult male rats increases coherent theta synchrony and directional connectivity between the dorsal CA1 region of the hippocampus and the prelimbic cortex. Optogenetic silencing of dorsal CA1 terminals in the prelimbic cortex during the reconsolidation induction window disrupted this theta coupling and led to delayed memory impairment. These findings demonstrate that reconsolidation depends on theta-mediated information transfer through the direct dorsal CA1-prelimbic pathway and suggest that monitoring or modulating this activity could inform the development of targeted interventions aimed to modify or disrupt distressing, intrusive memories.

KEYWORDS

hippocampus, prefrontal cortex, theta rhythm, coherence, synchrony, Granger causality, reconsolidation, fear memory, avoidance memory, amnesia

INTRODUCTION

Consolidated memories can become unstable upon reactivation and require protein synthesis-dependent reconsolidation to persist [1,2]. Disrupting this process may cause retrograde amnesia, making reconsolidation a target for treating anxiety disorders associated with maladaptive avoidance memory [3-5]. However, despite extensive research, the electrophysiological signature of reconsolidation remains poorly understood, limiting its clinical application.

During learning, the transfer of information between cooperating brain regions, such as the hippocampus and the medial prefrontal cortex (mPFC), is associated with changes in oscillatory activity, particularly in the theta band. Indeed, enhanced theta coherence between the CA1 region of the dorsal hippocampus (dCA1) and the prelimbic region of the mPFC (PrL) has been shown to support memory-guided decision-making [6,7], possibly through the dCA1→PrL monosynaptic pathway, which is also involved in learned fear expression and temporal order judgment [8,9].
Since dCA1 theta is engaged in avoidance memory reconsolidation only when reactivation triggers competing representations about the potential consequences of avoidance [10,11], and influences encoding in PrL as subjects switch memory strategies [7,12,13], we investigated whether avoidance memory reconsolidation affects theta connectivity between dCA1 and PrL, and how disrupting this connectivity impacts memory retention.

Our results show that, in adult male rats, avoidance memory reactivation increased direct dCA1→PrL theta connectivity during the induction of reconsolidation, and that optogenetically silencing dCA1 terminals in PrL disrupted this connectivity, leading to delayed amnesia. These findings indicate that reconsolidation depends on the transmission of theta-encoded information through the direct dCA1→PrL pathway, and suggest that monitoring theta synchrony between these brain regions during therapy may help predict the success of interventions aimed at modifying, erasing, or reframing avoidance memory.

RESULTS

Unreinforced SDIA-memory reactivation induces reconsolidation. To analyze the relationship between avoidance memory reconsolidation and dCA1/PrL theta interactions, we used the step-down inhibitory avoidance task (SDIA), a single-trial, fear-driven avoidance learning paradigm that engages both brain regions. In SDIA, rodents must suppress their innate tendency to step down from a platform to avoid a foot shock [14,15]. Unreinforced SDIA-memory reactivation induces dCA1-dependent reconsolidation, but only when the avoidance response is acquired in a familiar and safe environment [10,16], allowing for the differentiation of reconsolidation-specific mechanisms from those activated merely by memory recall. Thus, adult male Wistar rats with infusion cannulas and/or electrodes implanted in dCA1 and PrL were pre-exposed to the SDIA-training box for 5 min daily over 5 d to learn non-aversive information about the environment (PEX animals). This pre-exposure does not affect the future acquisition, strength, or persistence of SDIA-memory, but makes it susceptible to destabilization and hippocampus protein synthesis-dependent reconsolidation upon reactivation [11]. A separate group of rats, not pre-exposed to the SDIA-training box but handled for 5 min daily (HAN animals), served as a reconsolidation-resistant reactivation control. One day after the final pre-exposure or handling session, both groups were trained in SDIA and, the next day, they either underwent a 40 s manipulation to serve as no-reactivation controls (No RA) or experienced a 40 s unreinforced SDIA-memory reactivation session (RA). RA does not impact retention or facilitate extinction of the learned avoidance response but specifically induces SDIA-memory reconsolidation in PEX rats. Consistent with this, and confirming previous findings [10], analysis of SDIA-memory retention 1 d after RA showed that intra-dCA1 administration of the protein synthesis inhibitor anisomycin (ANI; 160 µg/side) 10 min post-RA induced amnesia only in PEX animals, not in HAN animals. ANI had no effect on SDIA-memory retention when administered 1 d post-training to either PEX or HAN rats that did not undergo RA (Fig. 1; $F(1,56) = 55.329$, $p = 6.529 \times 10^{-10}$ for pre-exposure; $F(1,56) = 42.848$, $p = 1.941 \times 10^{-8}$ for reactivation; $F(1,56) = 31.547$, $p = 6.333 \times 10^{-7}$ for post-RA treatment; $F(1,56) = 39.416$, $p = 5.222 \times 10^{-8}$ for pre-exposure/reactivation/treatment interaction in non-parametric three-way ART ANOVA [17]).

Reconsolidation enhances dCA1→PrL theta connectivity. Analysis of LFP data collected 10 min before, during, and 10 min after RA (Fig. 2A) revealed that theta power increased in the dCA1 of PEX animals during RA, returning to baseline after this session (Fig. 2B, left panel; $F(1,10) = 1.048$, $p = 0.3300$ for pre-exposure; $F(2,20) = 2.554$, $p = 0.1028$ for reactivation; $F(2,20) = 13.48$, $p = 0.0002$ for pre-exposure/reactivation interaction in two-way mixed-model design ANOVA). In contrast, theta power did not increase in the dCA1 of HAN animals or in the PrL of either group (Fig. 2B, right panel). Frequency spectra analysis showed increased mean and peak theta coherence between dCA1 and PrL during RA in PEX, but not in HAN animals, with coherence returning to baseline after the session (Fig. 2C; Mean theta coherence: $F(1,10) = 0.4892$, $p = 0.5002$ for pre-exposure; $F(2,20) = 6.938$, $p = 0.0051$ for reactivation; $F(2,20) = 6.527$, $p = 0.0064$ for pre-exposure/reactivation interaction in two-way mixed-model design ANOVA; Peak theta coherence: $F(1,10) = 1.232$, $p = 0.2930$ for pre-exposure; $F(2,20) = 8.752$, $p = 0.0019$ for reactivation; $F(2,20) = 8.206$, $p = 0.0025$ for pre-exposure/reactivation interaction in two-way mixed-model design ANOVA). This increased coherence persisted throughout RA (Fig. 2D), was independent of theta power fluctuations (Fig. 2E), and exhibited tight phase-locking (Fig. 2F; $F(1,10) = 3.153$, $p = 0.1062$ for pre-exposure; $F(2,20) = 11.47$, $p = 0.0005$ for reactivation; $F(2,20) = 5.010$, $p = 0.0172$ for pre-exposure/reactivation interaction in two-way mixed-model design ANOVA), suggesting enhanced functional theta coupling and high synchrony between dCA1 and PrL. Importantly, neither PEX nor HAN animals showed significant changes in delta (1 - 4 Hz), beta (15 - 25 Hz), slow gamma (35 - 55 Hz), or fast gamma (65 - 100 Hz) mean coherence or phase-locking values during RA (Fig. 2G). Spectral coherence analysis measures the efficiency of communication between brain regions or neuronal ensembles at specific oscillatory frequencies, while phase-locking analysis assesses the synchronicity of this coherence. However, neither method evaluates the directionality of oscillatory interactions. To address this, we used Granger causality (GC) analysis, a statistical tool that evaluates whether one time series is causal to another and can identify directional connectivity within specific frequency bands when applied in the frequency domain [18-20]. GC analysis revealed that RA was associated with a pronounced theta peak in the dCA1→PrL direction, but not in the PrL→dCA1 direction, only in PEX animals (Fig. 2H). The dCA1→PrL GC remained elevated throughout RA (Fig. 2I) but returned to baseline after this session (Fig. 2J; left panel: $F(1,10) = 8.696$, $p = 0.0146$ for pre-exposure; $F(2,20) = 9.045$, $p = 0.0016$ for reactivation; $F(2,20) = 5.198$, $p = 0.0152$ for pre-exposure/reactivation interaction in two-way mixed-model design ANOVA), suggesting that induction of SDIA-memory

reconsolidation enhances theta-encoded information flow from dCA1 to PrL. During RA, animals exhibited minimal movement (mean speed < 1 cm/s), thereby reducing speed-related influences on LFP activity. Furthermore, the procedures used for LFP data collection did not affect SDIA-memory retention in either PEX or HAN rats (Fig. 2K).

dCA1→PrL pathway inhibition impairs reconsolidation. We next investigated whether the monosynaptic pathway connecting dCA1 to PrL mediates the increase in directed theta connectivity triggered by reconsolidation, and whether this connectivity is necessary for the persistence of reactivated SDIA-memory. To confirm the existence of a direct dCA1→PrL connection [8], we injected naïve rats with the retrograde neuronal tracer cholera toxin B into PrL, which resulted in clear labeling in dCA1, as well as in dCA2/CA3 and the dentate gyrus (Fig. 3A and Fig. S1A). Additionally, we injected an adeno-associated virus vector carrying the yellow light-driven archaerhodopsin-T gene (AAV-CAG-ArchT-GFP) into dCA1, leading to distinct GFP-reported ArchT expression in PrL, anterior cingulate cortex, infralimbic cortex (Fig. 3B and Fig. S1B). Rats that received AAV-CAG-ArchT-GFP into dCA1 were then implanted with recording electrodes in both dCA1 and PrL (Fig. S2) and subjected to repeated pre-exposure to the SDIA-training box. These PEX rats were trained in SDIA and, 1 d later underwent RA. During this session, the animals either remained unstimulated or received light stimulation through optical fibers inserted into PrL (Fig. 3C). This allowed us to silence dCA1 terminals in PrL by illuminating PrL with yellow light, effectively deactivating the monosynaptic dCA1→PrL pathway. Blue light served as a nonspecific illumination control. We found that neither yellow nor blue light stimulation affected theta power in dCA1 (Fig. 3D, left panel; $F(2,13) = 0.1657$, $p = 0.8491$ for stimulation; $F(2,26) = 25.22$, $p < 0.0001$ for reactivation; $F(4,26) = 0.6001$, $p = 0.6659$ for stimulation/reactivation interaction in two-way mixed-model design ANOVA) or PrL (Fig. 3D, right panel). However, yellow light stimulation blocked the RA-induced increase in dCA1→PrL theta coherence (Fig. 3E, right panel; $F(2,13) = 4.505$, $p = 0.0326$ for stimulation; $F(2,26) = 20.15$, $p < 0.0001$ for reactivation; $F(4,26) = 4.626$, $p = 0.0059$ for stimulation/reactivation interaction in two-way mixed-model design ANOVA), phase-locking (Fig. 3F, right panel; $F(2,13) = 8.366$, $p = 0.0046$ for stimulation; $F(2,26) = 25.29$, $p < 0.0001$ for reactivation; and $F(4,26) = 2.777$, $p = 0.0480$ for stimulation/reactivation interaction in two-way mixed-model design ANOVA), and Granger causality (Fig. 3G; $F(2,13) = 7.261$, $p = 0.0076$ for stimulation; $F(2,26) = 15.82$, $p < 0.0001$ for reactivation; $F(4,26) = 3.154$, $p = 0.0307$ for stimulation/reactivation interaction in two-way mixed-model design ANOVA), resulting in amnesia during an SDIA-memory retention test session conducted 1 d post-RA (Fig. 3H; $H = 11.77$, $p = 0.0001$ in Kruskal-Wallis test). Importantly, yellow light PrL stimulation had no effect on SDIA-memory retention when applied 1 d after training to animals that did not undergo RA (Fig. 3I), or when it was delivered during RA, but retention was assessed 3 h instead of 1 d later (Fig. 3J). Additionally, yellow light PrL stimulation did not affect SDIA-memory retention when delivered during RA to SDIA-trained HAN animals injected with AAV-CAG-ArchT-GFP in dCA1 (Fig. 3K). Scatter plots illustrating the distribution of step-down latencies during the SDIA-memory retention test session, as a function of mean theta coherence and theta PLV during RA for the animals shown in Figs. 3C-H, suggest that stronger dCA1-PrL synchrony is associated with longer latencies (Fig. S3).

dCA1→PrL theta synchrony predicts memory retention. To further assess whether dCA1-PrL theta coherence during RA predicts step-down latency during the retention test, we applied a Cox proportional hazards regression model, accounting for right-censoring due to the 500 s ceiling. This approach allowed us to assess how coherence influences the hazard rate (i.e., the instantaneous probability of stepping down over time during the retention test). The analysis revealed a significant effect of dCA1-PrL theta coherence on step-down latency. The model estimate was -1.769, indicating that higher coherence values were associated with a lower hazard of stepping down. The corresponding hazard ratio (HR = 0.17) suggests that each unit increase in coherence reduced the risk of stepping down by approximately 83%. This effect was statistically significant, as confirmed by the generalized likelihood ratio test ($\chi^2(1) = 10.83$, $p = 0.0009$). The proportional hazards assumption was validated using the Schoenfeld test ($p = 0.7138$). Kaplan-Meier plots further illustrate that higher coherence during RA was associated with a greater probability of staying on the platform in the retention test session (Fig. 4A). Similarly, PLV significantly influenced step-down latency. Each unit increase in PLV during RA corresponded to a 64% reduction in the risk of stepping down at test (model estimate = -1.016, HR = 0.36, $\chi^2(1) = 8.73$, $p = 0.0031$). This effect also met the proportional hazards assumption, as confirmed by the Schoenfeld test ($p = 0.4288$). Kaplan-Meier plots showed that greater PLV during RA was associated with a higher probability of remaining on the platform throughout the retention test session (Fig. 4B).

DISCUSSION

Our data show that the induction of SDIA-memory reconsolidation requires enhanced theta-mediated communication from dCA1 to PrL, and suggest that this enhancement is not just a consequence of memory reactivation but a genuine marker of reconsolidation. This conclusion is supported by the finding that the RA-induced increase in synchronous theta activity between dCA1 and PrL occurred only in animals susceptible to reconsolidation. These animals were also the only ones to exhibit amnesia when the monosynaptic pathway linking dCA1 to PrL was inactivated during RA. The fact that this amnesia developed over time and did not occur when the direct dCA1→PrL pathway was deactivated in the absence of RA further supports the idea that dCA1→PrL theta connectivity drives a prolonged reconsolidation process essential for reactivated SDIA-memory maintenance.

Given that prior learning of non-aversive information about the training environment is crucial for SDIA-memory reconsolidation [10], it is reasonable to suggest that increased dCA1→PrL connectivity during RA reflects a struggle for behavioral control between two competing representations of potential avoidance consequences, which ultimately leads to the reconsolidation of the dominant representation, as predicted by the trace dominance hypothesis [21]. This view aligns with studies showing that the PrL regulates behavioral responses to contradictory information and modulates reactions to ambiguous cues during fear expression [22-26]. It also supports findings that theta synchrony between dCA1 and PrL increases during decision-making, facilitating network dynamics for comparing competing memories and resolving mismatches, thereby enabling behavioral flexibility [27,28]. Further evidence comes from previous work showing that chemogenetic inhibition of the dCA1→PrL pathway abolishes context retrieval-mediated fear memory enhancement induced by repeatedly re-exposing rats trained in a step-through passive avoidance task to the innately aversive lit compartment of the training box [8].
The potential to erase traumatic memories by blocking their reconsolidation has attracted significant interest [29,30], supported by extensive research in experimental animals [31,32]. However, despite some promising initial results, the effectiveness of reconsolidation-based therapies remains inconclusive [33,34], and a reliable biomarker for reconsolidation has not yet been identified. Our findings suggest that dCA1→PrL theta synchrony, easily measurable through non-invasive EEG connectivity analysis, could serve as a reliable biomarker for avoidance memory reconsolidation induction. This approach may help tailor memory reactivation protocols to individual patient needs, particularly for those with traumas or phobias linked to familiar contexts.

Limitations of the study

Since both conditioned fear and appetitive paradigms typically involve prior exposure to the training apparatus, exploring whether the dCA1→PrL pathway also plays a role in the reconsolidation of these memory types could offer insight on its broader function in memory stability and updating. Furthermore, given the higher prevalence of PTSD in women compared to men [35], future studies including female subjects will be crucial for evaluating the generalizability of our findings and identifying potential sex-specific mechanisms underlying avoidance memory reconsolidation.

RESOURCE AVAILABILITY

Lead contact

Further information and requests for resources and reagents should be directed to and will be fulfilled by the lead contact, Martin Cammarota (martin.cammarota@neuro.ufrn.br)

Materials availability

This study did not generate new unique reagents

Data and code availability

- Data reported in this study are available from the lead contact upon request.
- Code used in this study is available from the lead contact upon request.
- Any further information regarding the data or resources is available from the lead contact upon request.

ACKNOWLEDGMENTS

Supported by CNPq Grants 407459/2021-9 and 307433/2022-6, and CAPES grant code 001 to M.C. S.C.-O. current address is Netherlands Institute of Neuroscience, University of Amsterdam. We thank Dr. Thiago Z. de Lima for his help with the statistical analysis.

AUTHOR CONTRIBUTIONS

Conceptualization, M.C.; designed research, A.R., M.C.G., and M.C.; collected data, A.R., M.C.G., and J.I.R.; analyzed data, A.R., M.C.G., J.I.R., S.C.-O. and M.C.; funding acquisition, M.C.; project administration, M.C; supervision, M.C.; writing - original draft, M.C.; writing - review & editing, A.R., M.C.G., and M.C.

DECLARATION OF INTERESTS

The authors declare no competing interests.

DECLARATION OF GENERATIVE AI AND AI-ASSISTED TECHNOLOGIES

None.

SUPPLEMENTAL INFORMATION

Document S1. Figures S1-S3

FIGURE TITLES AND LEGENDS

Figure 1. SDIA-memory acquired in a familiar and safe environment is susceptible to hippocampus-dependent reconsolidation upon unreinforced reactivation. Schematic representation of the experimental protocol. Adult male Wistar rats were pre-exposed to the SDIA-training box (PEX) or handled (HAN) for 5 consecutive days. One day after the last pre-exposure or habituation session, rats were trained in the SDIA task (TR; 0.8 mA/2 s). The following day, rats were randomly assigned to two groups: one group underwent a 40 s unreinforced memory reactivation (RA) session, while the other group (No RA) was handled for 40 s and returned to their home cages. Ten min later, animals were randomly assigned to two subgroups, receiving bilateral intra-dCA1 infusions of either vehicle (VEH) or the protein synthesis inhibitor anisomycin (ANI; 160 µg/side). SDIA-memory retention was assessed 1 d later (TEST; n=8/group). Step-down latencies at TEST are presented as median ± IQR. **p < 0.01 in Wilcoxon pairwise comparisons with Bonferroni correction after three-way ART ANOVA.

Figure 2. Induction of SDIA-memory reconsolidation increases dCA1→PrL theta connectivity. (A) The left panel illustrates the experimental protocol. Adult male Wistar rats were pre-exposed to the SDIA-training box (PEX) or handled (HAN) for 5 consecutive days. One day after the last session, rats were trained in the SDIA task (TR; 0.8 mA/2 s). The next day, animals underwent a 40 s unreinforced memory reactivation (RA) session, during which local field potentials (LFPs) from dCA1 and PrL were recorded. LFPs were also recorded approximately 10 min before (Pre_{RA}) and after RA ($Post_{RA}$) in a familiar recording cage. Only the first 40 s of stable awake signals with minimal movement were used for analysis. SDIA-memory retention was assessed 1 d later (TEST). The right panel shows raw dCA1 and PrL LFP recordings, with filtered theta (5-10 Hz) data from a PEX animal during RA. (B) dCA1 and PrL theta power calculated before, during, and after RA. (C) dCA1-PrL spectral coherence, mean theta coherence, and peak theta coherence calculated before, during, and after RA. (D) CA1-PrL coherogram during RA for PEX animals. (E) dCA1-PrL mean theta coherence, dCA1 theta power, and PrL theta power calculated in non-overlapping 1 s epochs during RA for PEX animals. (F) dCA1-PrL phase-locking values (PLV) during RA, along with theta PLV calculated before, during, and after RA. (G) dCA1-PrL mean coherence and PLV calculated before, during, and after RA for delta (1 - 4 Hz), beta (15 - 25 Hz), slow-gamma (35 - 55 Hz), and fast-gamma (65 - 100 Hz) frequency bands. (H) dCA1→PrL and PrL→dCA1 spectral Granger causality (GC) during RA. (I) dCA1→PrL and PrL→dCA1 grangerograms during RA. (J) dCA1→PrL and PrL→dCA1 theta GC calculated before, during, and after RA. (K) Step-down latencies at TEST (n=6/group). Data are expressed as mean ± SEM or median ± IQR. **p < 0.01 and ***p < 0.001 in Bonferroni test after two-way mixed model design ANOVA.

Figure 3.Optogenetic silencing of the dCA1→PrL monosynaptic pathway during SDIA-memory reactivation impairs reconsolidation and causes delayed amnesia. (A) Representative images showing dCA1 CTB-labeling (red) following intra-PrL CTB injection, with labeled cells in dCA1 indicated by white arrowheads. (B) Representative images showing GFP-reported ArchT expression (green) in dCA1 and PrL following intra-dCA1 AAV-CAG-ArchT-GFP injection, with labeled projections in PrL indicated by white arrowheads. (C) Experimental protocol schematic. Adult male Wistar rats injected with AAV-CAG-ArchT-GFP into dCA1 and implanted with electrodes in dCA1 and PrL, as well as optical fibers in the PrL, were exposed to the step-down inhibitory avoidance (SDIA) training box for 5 consecutive days (5 min sessions; PEX). One day after the last session, the animals were trained in the SDIA task (TR; 0.8 mA/2 s), and the next day they were randomly assigned to three experimental groups and underwent a 40 s unreinforced memory reactivation (RA) session. During this session, one group of animals remained unstimulated (Off), while the others received PrL stimulation with either yellow or blue light. Local field potentials (LFPs) from dCA1 and PrL were recorded before (Pre_{RA}), during, and after RA ($Post_{RA}$). Memory retention was evaluated 1 d later (TEST). (D) dCA1 and PrL theta (5-10 Hz) power calculated before, during, and after RA. (E) dCA1-PrL spectral coherence and mean theta coherence calculated before, during, and after RA. (F) dCA1-PrL phase-locking values (PLV) during RA and theta PLV calculated before, during, and after RA. (G) dCA1→PrL Granger causality (GC) during RA, theta GC calculated before, during, and after RA, and dCA1→PrL grangerograms during RA. (H) Step-down latencies at TEST for animals in B-G (Off: n = 5; Yellow: n = 6; Blue: n = 5). (I) SDIA-trained PEX animals injected with AAV-CAG-ArchT-GFP in dCA1 were unstimulated (Off) or stimulated with yellow or blue light in PrL for 40 s while exploring a familiar, non-aversive box (No RA). Memory retention was evaluated 1 d later (n = 7/group). (J) SDIA-trained PEX animals injected with AAV-CAG-ArchT-GFP in dCA1 were unstimulated (Off) or stimulated with yellow or blue light in PrL during RA. Memory retention was evaluated 3 h later (n = 7/group). (K) SDIA-trained HAN animals injected with AAV-CAG-ArchT-GFP in dCA1 and implanted with optic fibers in PrL were unstimulated (Off) or stimulated with yellow or blue light in PrL during a 40 s unreinforced memory reactivation session (RA). Memory retention was evaluated 1 d later (TEST; n = 7/group). Data are expressed as mean ± SEM or median ± IQR. *p < 0.05, **p < 0.01, ***p < 0.001 in Bonferroni multiple comparison test after two-way mixed-model design ANOVA or Dunn's post-hoc test following Kruskal-Wallis. See also Figures S1-S3.

Figure 4. Theta synchrony between dCA1 and PrL during RA predicts future SDIA-memory retention. Cox proportional hazards regression assessing the impact of dCA1-PrL theta synchrony during the reactivation session, measured as theta coherence or PLV, on step-down latency during the retention test session for the animals shown in Figs. 3C-H.

STAR★METHODS

EXPERIMENTAL MODEL AND SUBJECT DETAILS

Animals

We used three-month-old male Wistar rats (Rattus norvegicus; RRID: RGD_13508588) weighing 300-350 g. The animals were housed in groups of 4-5 per cage in ventilated racks, with ad libitum access to food and water. The animal facility maintained a controlled environment with temperatures ranging from 22-23°C and a standard 12 h light/dark cycle (lights on at 6:00 AM, lights off at 6:00 PM). Naïve littermates were randomly assigned to experimental groups. All procedures were performed in accordance with the National Institutes of Health (NIH) Guide for the Care and Use of Laboratory Animals and followed the ARRIVE guidelines. The study protocol was approved by the local ethics committee (Comissão de Ética no Uso de Animais, Universidade Federal do Rio Grande do Norte).

METHODS DETAILS

Surgical procedures

Stereotaxic surgeries for implantations and AAV infusions were performed under anesthesia with ketamine (80 mg/kg) and xylazine (10 mg/kg). Coordinates were determined relative to Bregma, based on previous reports. For intra-dCA1 drug administration, stainless steel guide cannulas (22-G) were bilaterally implanted at the following coordinates: AP −4.2 mm, LL ±3.0 mm, and DV −2.0 mm [36]. LFP signals were recorded using single tungsten wire field electrodes (50 µm) placed in the dCA1 (AP, −4.2 mm; LL, +3 mm; DV, −3 mm) and in the PrL (AP, +3.2 mm; LL, +0.8; DV,

-3.5 mm) [14, 15]. A screw was inserted into the parietal bone to establish a ground connection. To confirm the monosynaptic pathway from dCA1 to PrL, the retrograde tracer recombinant cholera toxin subunit B conjugated to CF568 (CTB-568; Biotium #00071) was injected into the PrL (AP, +3.2 mm; LL, +0.8 mm; DV, -3.5 mm) using a Hamilton syringe and infusion pump (0.5 µl; infusion rate: 0.1 µl/min). For optogenetic silencing of the dCA1→PrL pathway, the adeno-associated viral vector AAV-CAG-ArchT-GFP (UNC Vector Core; 2×10^{11} particles/ml) was delivered along the lateral axis of dCA1 (AP, −4.2 mm; LL, +2.5/+3/+3.5 mm; DV, −3 mm) using a Hamilton syringe and infusion pump (3 injections of 0.5 µl; infusion rate: 0.1 µl/min). Three weeks later, fiber optic cannulas or optotrodes were bilaterally implanted into PrL (AP, +3.2 mm; LL, +/-0.8; DV, -3.5 mm). The optotrodes, consisting of single tungsten wire electrodes (50 µm) glued to a 200 µm optical fiber with a ferrule [37], were positioned such that the fiber tip was ~0.5 mm above the electrode tips. In addition, single tungsten wire field electrodes (50 µm) were also implanted into the dCA1 (AP, −4.2 mm; LL, +3 mm; DV, −3 mm). All implants were secured to the skull with auto-polymerizing dental resin. Postoperatively, rats were given meloxicam (0.2 mg/kg) for pain management and allowed a recovery period of 7 - 10 d before behavioral procedures.

Step-down inhibitory avoidance task

The animals were habituated to the headstage and/or optical fiber connection, allowing them to move freely in a recording cage with cables attached to the implants. The step-down inhibitory avoidance (SDIA) training box (50 cm × 25 cm × 25 cm), made of Plexiglas, featured a grid floor capable of delivering scrambled electric shocks. A wooden platform (8 cm × 25 cm × 5 cm) was placed at the left end of the grid floor. Prior to training, rats underwent either handling (HAN animals) or were placed on the SDIA training box platform to explore the box freely for 5 min daily for 5 consecutive days (PEX animals). During training (TR), animals were positioned on the platform, facing the left rear corner of the box. When they stepped down onto the grid floor with all four paws, they received a 2 s, 0.8 mA scrambled foot shock. Immediately after the shock, they were removed from the apparatus. One day after TR, rats were placed back on the platform for 40 s to reactivate SDIA memory (reactivation session, RA). They remained on the platform for the full session and were returned to their home cages afterward. SDIA memory retention was assessed 1 d after RA (TEST session), except in one experiment where the TEST session occurred 3 h after RA. During TEST, the animals were placed back on the training box platform and the latency to step down onto the grid was measured. The session ended either when the animal stepped down or after a maximum of 500 s, with no foot shock administered. Each animal underwent only one training and testing session.

Drug administration

The protein synthesis inhibitor anisomycin (ANI; 160 µg/side; Sigma-Aldrich #A9789) was purchased from Merck/Sigma-Aldrich. The dose used was based on previous studies. Intra-dCA1 infusions were performed using injectors that extended 1 mm beyond the guide cannulas. The injectors were connected to Hamilton syringes via polyethylene tubes. Drug delivery (1 µl per side) was controlled with an infusion pump at a rate of 0.1 µl/min, with the injectors left in place for 1 to 2 min. After the completion of the experiments, the positions of the cannulas were verified. To confirm accurate infusion placement, 4% methylene blue (1 µl) was injected into dCA1. Animals were then euthanized, and their brains were extracted and analyzed for dye diffusion, which helped verify the spread of the drug or vehicle. Animals with misplaced cannula implants (3% of the total sample) were excluded from statistical analysis.

Optogenetic stimulation

Blue (470 nm) or yellow (565 nm) light was delivered bilaterally to the PrL using LEDs controlled by a DC4104 LED driver (ThorLabs Inc.). Light stimulation (5 mW measured at the fiber tip) was applied continuously for 40 s during the reactivation session (RA) in the SDIA training box or while animals explored a familiar, non-aversive box.

Electrophysiological recordings and analysis

Signals were acquired at 1 kHz, filtered (pass band 0.3 to 250 Hz), amplified, digitized, and stored using the Cerebus Neural Signal Processor system (Blackrock Neurotech). Data analysis was performed in MATLAB (RRID: SCR_001622). LFP data were detrended ('detrend' function) to remove non-neuronal, slow-changing components that could distort signals [38] and cause an overall shift of the spectrum, resulting in incorrect power estimates. Subsequently, data were z-score normalized using the 'zscore' function. Power spectra were computed using Welch's method with the 'pwelch' function, applying 1 s Hamming windows and 50% overlap. Theta band power (5-10 Hz) was defined as the average power obtained by integrating the power spectral

density within this frequency range using the 'bandpower' function. Coherence analysis was conducted using the 'mscohere' function to estimate magnitude-squared coherence between two input signals (x and y) via Welch's method. Coherograms were generated using 6 s windows and 850 ms steps. Phase coupling was assessed using the phase-locking value (PLV). Given the phase time series θ1 and θ2, estimated from two different oscillations (i.e., band-pass filtered signals from the dCA1 and PrL) with N samples and frequency f, PLV was defined as: $PLV(f) = \frac{1}{N}\left|\sum_{n=1}^{N} e^{i(\theta_{1nf}-\theta_{2nf})}\right|$.

To estimate phase time series (θ1 and θ2), LFP signals were detrended and filtered within the theta frequency range using the 'eegfilt.m' function. Phase time series were then calculated by taking the angle of the Hilbert transform of the filtered signals. Granger causality was estimated using the Multivariate Granger Causality MATLAB toolbox [39]. All LFP traces were down sampled to 125 Hz and z-score normalized before analysis. The order of the variational autoregressive model was set to 15 and pairwise conditional spectral Granger causality was computed with a frequency resolution of 0.25 Hz. Statistical significance was assessed using F-tests, with α = 0.05. Granger causality was calculated over 10 consecutive, non-overlapping 4 s windows to assess its variation over time. For each animal, Granger causality as a function of time and frequency [40] was normalized to the maximum value for that animal. Recordings were made during RA in the SDIA-training box and in a familiar recording cage, 10 min before and 10 min after RA. Behavior was recorded using video cameras (30 frames/s) positioned above the experimental boxes and analyzed with the TopScan system (RRID: SCR_017141). For pre-RA and post-RA analysis, only the first 40 s of stable signals, when the animal was awake and exhibited minimal movement, were used. During RA, animals remained still on the platform (mean speed < 1 cm/s), thus minimizing the potential influence of speed-dependent variations in dCA1 and PrL LFP activity on the results. Anatomical localization of the electrodes was confirmed through LFP features and histologic verification of the electrode tracks [41,42].

CTB analysis and immunofluorescence

Animals were anesthetized with an overdose of thiopental and transcardially perfused with heparinized saline (0.9% NaCl) followed by 4% paraformaldehyde (PFA). Brains were extracted, post-fixed in PFA at 4°C overnight, and transferred to 30% sucrose at 4°C for 48 h. Coronal sections (50 µm) were prepared using a cryostat. For CTB analysis, sections were rinsed with PBS, stained with DAPI (1:1000; RRID: AB_2629482), and mounted using Fluoromount-G (RRID: SCR_015961). For AAV-CAG-ArchT-GFP expression analysis, sections were rinsed in PBS, incubated in PBST (0.2% Triton X-100) for 1 h, and blocked with 10% normal goat serum (NGS) in PBST for 2 h at room temperature. Sections were then incubated overnight at 4°C with anti-GFP antibody (1:1000; RRID: AB_91337), rinsed with PBST, and incubated with goat anti-rabbit Alexa Fluor 488-conjugated antibody (1:1000; RRID: AB_143165) for 3 h at room temperature. After rinsing in PBS, sections were stained with DAPI, and mounted with Fluoromount-G. Images were captured using a Zeiss Axio Imager-Z2 fluorescence microscope (RRID: SCR_018856) and a Zeiss LSM 710 confocal microscope system (RRID: SCR_018063; Black Zen software, RRID: SCR_018163). To quantify CTB+ cells in dorsal CA1, CA2/3, and dentate gyrus (DG), corrected total cellular fluorescence (CTCF) was calculated using the formula: CTCF = Integrated Density – (Area of selected tissue × Mean background fluorescence) [43,44]. This approach accounts for background signal by subtracting background fluorescence from the integrated fluorescence intensity. Normalized CTCF was then computed as: Normalized CTCF = CTCF / Total Area. To assess GFP+ projections in the cingulate cortex, prelimbic cortex, and infralimbic cortex, we used the Area Fraction Fractionator probe within the Stereo Investigator software (version 11; MicroBrightField Bioscience, RRID: SCR_002526). This method, based on the Cavalieri point counting technique, provides unbiased estimates of area and volume [45,46]. Sampling parameters included a grid size of 250 µm × 250 µm, a counting frame of 250 µm × 250 µm, and a grid spacing of 10 µm. Cortical regions were delineated under x5 magnification and GFP+ projections were analyzed at x20 magnification. The area fraction for each region was calculated as: Area of GFP+ projections / Total Area.

QUANTIFICATION AND STATISTICAL ANALYSIS

Statistical analyzes were performed using GraphPad Prism 8 (RRID:SCR_002798) and RStudio (RRID:SCR_000432). Given the 500 s limit on step-down latencies during the test session, nonparametric statistical methods were used. For SDIA data, we used three-way aligned rank transform (ART) ANOVA followed by Wilcoxon pairwise comparisons with Bonferroni correction,

or the Kruskal-Wallis test followed by Dunn's post-hoc comparisons. Electrophysiological data were analyzed using a two-way mixed-model design ANOVA followed by Bonferroni post-hoc comparisons. The significance level was set at $\alpha = 0.05$, and the sample sizes determined based on previous studies. The Cox proportional hazards model, a generalized likelihood ratio test and Kaplan–Meier plots were used to analyze the relationship between the strength of theta synchrony during the reactivation session and step-down latencies observed during the SDIA-memory test session [47]. In the figures, dots represent individual subjects per group. Researchers were blinded to the treatment conditions during data collection and analysis.

REFERENCES

1. Przybyslawski, J., Sara, S.J. (1997). Reconsolidation of memory after its reactivation. Behav. Brain Res. 84, 241-246. doi:10.1016/S0166-4328(96)00153-2.

2. Nader, K., Schafe, G.E., LeDoux, J.E. (2000). Fear memories require protein synthesis in the amygdala for reconsolidation after retrieval. Nature 406, 722-726. doi:10.1038/35021052.

3. Nader, K. (2015). Reconsolidation and the dynamic nature of memory. Cold Spring Harb. Perspect. Biol. 7, a021782. doi:10.1101/cshperspect.a021782.

4. Kida, S. (2019). Reconsolidation/destabilization, extinction, and forgetting of fear memory as therapeutic targets for PTSD. Psychopharmacology 236, 49-57. doi:10.1007/s00213-018-5086-2.

5. Bui, U.T.D., Milton, A.L. (2023). Making leaps and hitting boundaries in reconsolidation: Overcoming boundary conditions to increase clinical translatability of reconsolidation-based therapies. Neuroscience 519, 198-206. doi:10.1016/j.neuroscience.2023.03.013.

6. Shin, J.D., Tang, W., Jadhav, S.P. (2019). Dynamics of awake hippocampal-prefrontal replay for spatial learning and memory-guided decision making. Neuron 104, 1110-1125.e7. doi:10.1016/j.neuron.2019.09.012.

7. Zielinski, M.C., Shin, J.D., Jadhav, S.P. (2019). Coherent coding of spatial position mediated by theta oscillations in the hippocampus and prefrontal cortex. J. Neurosci. 39, 4550-4565. doi:10.1523/JNEUROSCI.0106-19.2019.

8. Ye, X., Kapeller-Libermann, D., Travaglia, A., Inda, M.C., Alberini, C.M. (2017). Direct dorsal hippocampal-prelimbic cortex connections strengthen fear memories. Nat. Neurosci. 20, 52-61. doi:10.1038/nn.4472.

9. Barker, G.R., Banks, P.J., Scott, H., Ralph, G.S., Mitrophanous, K.A., Wong, L.F., Bashir, Z.I., Uney, J.B., Warburton, E.C. (2017). Separate elements of episodic memory subserved by distinct hippocampal-prefrontal connections. Nat. Neurosci. 20, 242-250. doi:10.1038/nn.4472.

10. Radiske, A., Gonzalez, M.C., Conde-Ocazionez, S.A., Feitosa, A., Köhler, C.A., Bevilaqua, L.R., Cammarota, M. (2017). Prior learning of relevant nonaversive information is a boundary condition for avoidance memory reconsolidation in the rat hippocampus. J. Neurosci. 37, 9675-9685. doi:10.1523/JNEUROSCI.1372-17.2017.

11. Radiske, A., Gonzalez, M.C., Conde-Ocazionez, S., Rossato, J.I., Köhler, C.A., Cammarota, M. (2020). Cross-frequency phase-amplitude coupling between hippocampal theta and gamma oscillations during recall destabilizes memory and renders it susceptible to reconsolidation disruption. J. Neurosci. 40, 6398-6408. doi:10.1523/JNEUROSCI.0259-20.2020.

12. Shin, J.D., Jadhav, S.P. (2016). Multiple modes of hippocampal-prefrontal interactions in memory-guided behavior. Curr. Opin. Neurobiol. 40, 161-169. doi:10.1016/j.conb.2016.07.015.

13. Backus, A.R., Schoffelen, J.M., Szebényi, S.S., Hanslmayr, C.F. (2016). Hippocampal-Prefrontal Theta Oscillations Support Memory Integration. Curr. Biol. 26, 450-457. doi: 10.1016/j.cub.2015.12.048.

14. Luft, T., Pereira, G.S., Cammarota, M., Izquierdo, I. (2004). Different time course for the memory facilitating effect of bicuculline in hippocampus, entorhinal cortex, and posterior parietal cortex of rats. Neurobiol. Learn. Mem. 82, 52-56. doi:10.1016/j.nlm.2004.03.002.

15. Paratcha, G., Furman, M., Bevilaqua, L., Cammarota, M., Vianna, M., de Stein, M.L., Izquierdo, I., Medina, J.H. (2000). Involvement of hippocampal PKCbetaI isoform in the early

phase of memory formation of an inhibitory avoidance learning. Brain Res. 855, 199-205. doi:10.1016/S0006-8993(99)02323-9.

16. Radiske, A., Gonzalez, M.C., Rossato, J.I., Apolinário, G., de Oliveira, J.R., Bevilaqua, L.R., Cammarota, M. (2021). Avoidance memory requires CaMKII activity to persist after recall. Mol. Brain 14, 167. doi:10.1186/s13041-021-00877-5.

17. Oliver-Rodríguez, J.C., Wang, X.T. (2015). Non-parametric three-way mixed ANOVA with aligned rank tests. Br. J. Math. Stat. Psychol. 68, 23-42. doi:10.1111/bmsp.12031.

18. Liu, S., Molenaar, P. (2016). Testing for Granger Causality in the Frequency Domain: A Phase Resampling Method. Multivariate Behav. Res. 51, 53-66. doi:10.1080/00273171.2015.1100528.

19. Shojaie, A., Fox, E.B. (2022). Granger Causality: A Review and Recent Advances. Annu. Rev. Stat. Appl. 9, 289-319. doi:10.1146/annurev-statistics-040120-010930.

20. Seth, A.K., Barrett, A.B., Barnett, L. (2015). Granger causality analysis in neuroscience and neuroimaging. J. Neurosci. 35, 3293-3297. doi:10.1523/JNEUROSCI.4399-14.2015.

21. Eisenberg, M., Kobilo, T., Berman, D.E., Dudai, Y. (2003). Stability of retrieved memory: inverse correlation with trace dominance. Science 301, 1102–1104. doi:10.1126/science.1086881.

22. Fernandez-Leon, J.A., Engelke, D.S., Aquino-Miranda, G., Goodson, A., Rasheed, M.N., Do Monte, F.H. (2021). Neural correlates and determinants of approach-avoidance conflict in the prelimbic prefrontal cortex. Elife 10, e74950. doi:10.7554/eLife.74950.

23. Niedringhaus, M., West, E.A. (2022). Prelimbic cortex neural encoding dynamically tracks expected outcome value. Physiol. Behav. 256, 113938. doi:10.1016/j.physbeh.2022.113938.

24. Giannotti, G., Heinsbroek, J.A., Yue, A.J., Deisseroth, K., Peters, J. (2019). Prefrontal cortex neuronal ensembles encoding fear drive fear expression during long-term memory retrieval. Sci. Rep. 9, 10709. doi:10.1038/s41598-019-47095-7.

25. Marquis, J.P., Killcross, S., Haddon, J.E. (2007). Inactivation of the prelimbic, but not infralimbic, prefrontal cortex impairs the contextual control of response conflict in rats. Eur. J. Neurosci. 25, 559-566. doi:10.1111/j.1460-9568.2006.05295.x.

26. Sharpe, M.J., Killcross, S. (2015). The prelimbic cortex directs attention toward predictive cues during fear learning. Learn. Mem. 22, 289-293.

27. Tang, W., Shin, J.D., Jadhav, S.P. (2021). Multiple time-scales of decision making in the hippocampus and prefrontal cortex. Elife 10, e70438. doi:10.7554/eLife.70438.

28. Hyman, J.M., Hasselmo, M.E., Seamans, J.K. (2011). What is the Functional Relevance of Prefrontal Cortex Entrainment to Hippocampal Theta Rhythms? Front. Neurosci. 5, 24. doi:10.3389/fnins.2011.00024.

29. Nader, K., Einarsson, E.O. (2010). Memory reconsolidation: an update. Ann. N.Y. Acad. Sci. 1191, 27-41. doi:10.1111/j.1749-6632.2010.05443.x.

30. Wang, S.H. (2022). Lose the fear and boost the everyday memory through memory destabilisation and reconsolidation. Brain Res. Bull. 190, 134-139. doi:10.1016/j.brainresbull.2022.09.019.

31. Bellfy, L., Kwapis, J.L. (2020). Molecular Mechanisms of Reconsolidation-Dependent Memory Updating. Int. J. Mol. Sci. 21, 6580. doi:10.3390/ijms21186580.

32. Gonzalez, M.C., Radiske, A., Cammarota, M. (2019). On the Involvement of BDNF Signaling in Memory Reconsolidation. Front. Cell. Neurosci. 13, 383. doi:10.3389/fncel.2019.00383.

33. Dunbar, A.B., Taylor, J.R. (2017). Reconsolidation and psychopathology: Moving towards reconsolidation-based treatments. Neurobiol. Learn. Mem. 142, 162-171. doi:10.1016/j.nlm.2016.11.005.

34. Elsey, J.W.B., Van Ast, V.A., Kindt, M. (2018). Human memory reconsolidation: A guiding framework and critical review of the evidence. Psychol. Bull. 144, 797-848. doi:10.1037/bul0000152.

35. Ressler, K.J., Berretta, S., Bolshakov, V.Y., Rosso, I.M., Meloni, E.G., Rauch, S.L., Carlezon, W.A. Jr. (2022). Post-traumatic stress disorder: clinical and translational neuroscience from cells to circuits. Nat Rev Neurol. 18(5):273-288. doi: 10.1038/s41582-022-00635-8.

36. Rossato, J. I., Köhler, C. A., Radiske, A., Bevilaqua, L. R., and Cammarota, M. (2015). Inactivation of the dorsal hippocampus or the medial prefrontal cortex impairs retrieval but has differential effect on spatial memory reconsolidation. Neurobiol. Learn. Mem. 125, 146–151. doi:10.1016/j.nlm.2015.09.001.

37. Mikulovic, S., Restrepo, C. E., Siwani, S., Bauer, P., Pupe, S., Tort, A. B. L., Kullander, K., and Leão, R. N. (2018). Ventral hippocampal OLM cells control type 2 theta oscillations and response to predator odor. Nat. Commun. 9(1), 3638. doi:10.1038/s41467-018-05907-w.

38. van der Meer, M.A., Redish, A.D. (2011). Theta phase precession in rat ventral striatum links place and reward information. J Neurosci. 31(8):2843-54. doi: 10.1523/JNEUROSCI.4869-10.2011.

39. Barnett, L., and Seth, A. K. (2014). The MVGC multivariate Granger causality toolbox: a new approach to Granger-causal inference. J. Neurosci. Methods 223, 50–68. doi:10.1016/j.jneumeth.2013.10.018.

40. Tavares, L. C. S., and Tort, A. B. L. (2022). Hippocampal-prefrontal interactions during spatial decision-making. Hippocampus 32(1), 38–54. doi:10.1002/hipo.23394.

41. Brankack, J., Stewart, M., and Fox, S. E. (1993). Current source density analysis of the hippocampal theta rhythm: associated sustained potentials and candidate synaptic generators. Brain Res. 615(2), 310–327. doi:10.1016/0006-8993(93)90043-m.

42. Bragin, A., Jandó, G., Nádasdy, Z., Hetke, J., Wise, K., and Buzsáki, G. (1995). Gamma (40-100 Hz) oscillation in the hippocampus of the behaving rat. J. Neurosci. 15(1 Pt 1), 47–60. doi:10.1523/JNEUROSCI.15-01-00047.1995.

43. Baptista-de-Souza, D., Tavares-Ferreira, D., Megat, S., Sankaranarayanan, I., Shiers, S., Flores, C.M., Ghosh, S., Luiz Nunes-de-Souza, R., Canto-de-Souza, A., Price, T.J. (2020). Sex differences in the role of atypical PKC within the basolateral nucleus of the amygdala in a mouse hyperalgesic priming model. Neurobiol Pain, 8, 100049. doi:10.1016/j.ynpai.2020.100049.

44. Harris, L., Rigo, P., Stiehl, T., Gaber, Z.B., Austin, S.H.L., Masdeu, M.D.M., Edwards, A., Urbán, N., Marciniak-Czochra, A., Guillemot, F. (2021). Coordinated changes in cellular behavior ensure the lifelong maintenance of the hippocampal stem cell population. Cell Stem Cell, 28(5), 863-876.e6. doi:10.1016/j.stem.2021.01.003.

45. Oñate-Ponce, A., Muñoz-Muñoz, C., Catenaccio, A., Court, F.A., Henny, P. (2024). Applying the area fraction fractionator (AFF) probe for total volume estimations of somatic, dendritic and axonal domains of the nigrostriatal dopaminergic system in a murine model. J Neurosci Methods, 410, 110226. doi:10.1016/j.jneumeth.2024.110226.

46. McBride, J.L., Pitzer, M.R., Boudreau, R.L., Dufour, B., Hobbs, T., Ojeda, S.R., Davidson, B.L. (2011). Preclinical safety of RNAi-mediated HTT suppression in the rhesus macaque as a potential therapy for Huntington's disease. Mol Ther, 19(12), 2152-2162. doi:10.1038/mt.2011.219.

47. Cox, D.R. (1972). Regression models and life-tables. J R Stat Soc Series B Methodol, 34(2), 187–220. doi: 10.1111/j.2517-6161.1972.tb00899.x

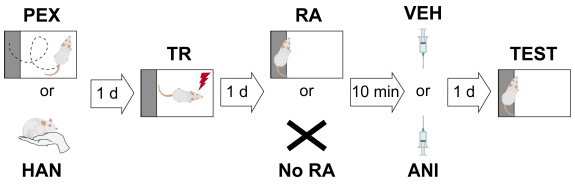

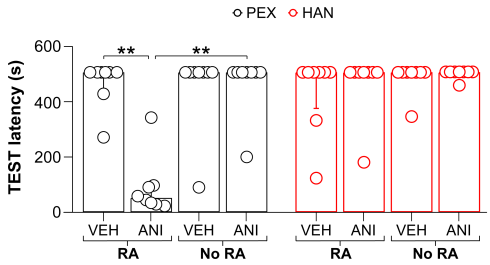

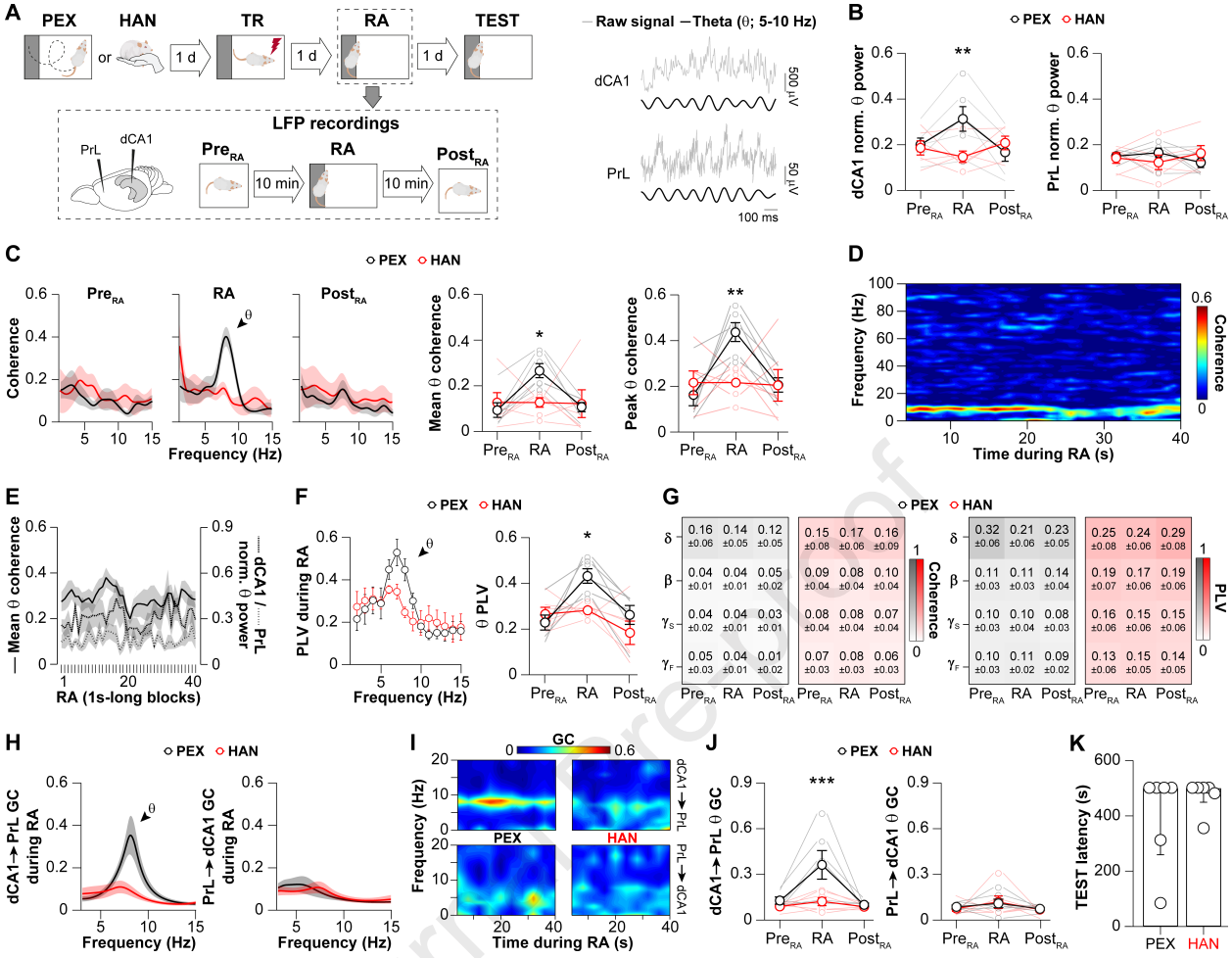

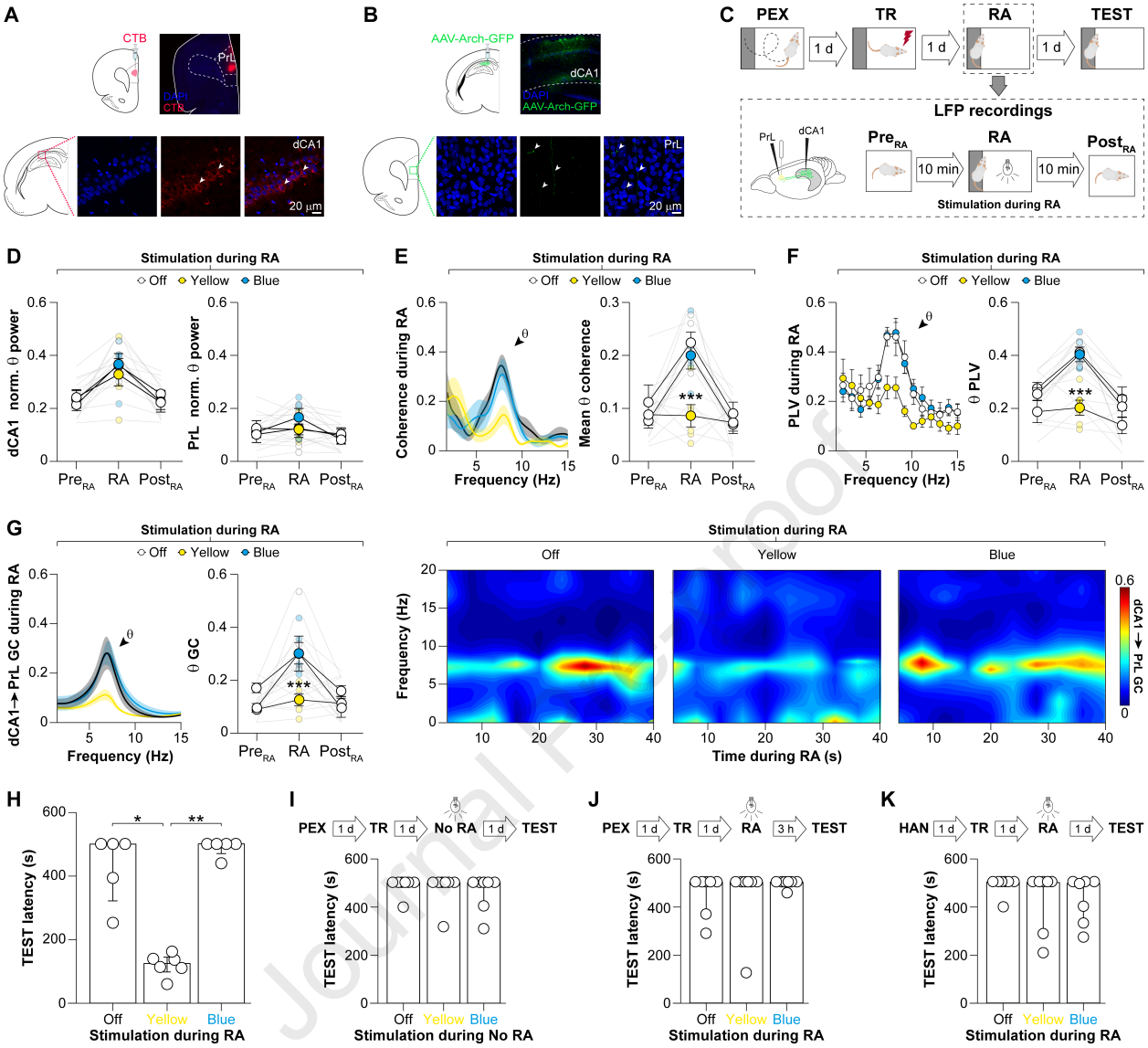
A
CTB
PrL
DAPI
CTB
dCA1
20 μm
B
AAV-Arch-GFP
dCA1
DAPI
AAV-Arch-GFP
PrL
20 μm
C
PEX
TR
RA
TEST
1 d
1 d
1 d
LFP recordings
PrL
dCA1
Pre_RA
10 min
RA
10 min
Post_RA
Stimulation during RA
D
Stimulation during RA
Off
Yellow
Blue
dCA1 norm. θ power
PrL norm. θ power
Pre_RA
RA
Post_RA
E
Stimulation during RA
Off
Yellow
Blue
Coherence during RA
θ
Frequency (Hz)
Mean θ coherence
***
Pre_RA
RA
Post_RA
F
Stimulation during RA
Off
Yellow
Blue
PLV during RA
θ
Frequency (Hz)
θ PLV
***
Pre_RA
RA
Post_RA
G
Stimulation during RA
Off
Yellow
Blue
dCA1→PrL GC during RA
θ
Frequency (Hz)
θ GC
***
Pre_RA
RA
Post_RA
Stimulation during RA
Off
Yellow
Blue
Frequency (Hz)
Time during RA (s)
dCA1→PrL GC
H
TEST latency (s)
*
**
Off
Yellow
Blue
Stimulation during RA
I
PEX
1 d
TR
1 d
No RA
1 d
TEST
TEST latency (s)
Off
Yellow
Blue
Stimulation during No RA
J
PEX
1 d
TR
1 d
RA
3 h
TEST
TEST latency (s)
Off
Yellow
Blue
Stimulation during RA
K
HAN
1 d
TR
1 d
RA
1 d
TEST
TEST latency (s)
Off
Yellow
Blue
Stimulation during RA

A

θ coherence

Estimate	Loglik	Chisq	DF	p
-1.769	-16.72	10.83	1	0.0009

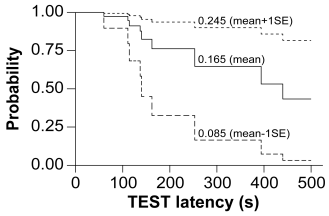

B

θ PLV

Estimate	Loglik	Chisq	DF	p
-1.016	-17.77	8.73	1	0.0031

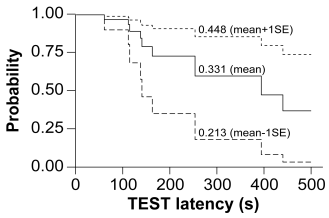

HIGHLIGHTS

- Reactivation causes avoidance memory reconsolidation only if learnt in a safe context
- Avoidance memory reconsolidation increases dCA1→PrL theta synchrony
- dCA1→PrL theta synchrony during reactivation predicts avoidance memory retention
- Silencing dCA1→PrL theta flow blocks reconsolidation and causes amnesia

Key resources table

REAGENT or RESOURCE	SOURCE	IDENTIFIER
Antibodies		
Anti-Green Fluorescent Protein	Millipore	Cat# AB3080, RRID: AB_91337
Goat anti-Rabbit Alexa Fluor™ 488	Thermo Fisher Scientific	Cat# A-11008, RRID: AB_143165
Chemicals, peptides, and recombinant proteins		
Anisomycin	Sigma-Aldrich	Cat# A9789
Cholera Toxin Subunit B CF®568	Biotium, Inc.	Cat# 00071
DAPI (4',6-Diamidino-2-Phenylindole, Dihydrochloride)	Thermo Fisher Scientific	RRID: AB_2629482
ProLong. Fluoromount G Mounting Medium	Thermo Fisher Scientific	RRID: SCR_015961
Experimental models: Organisms/strains		
Male Wistar rats	Federal University of Rio Grande do Norte	RRID: RGD_13508588
Software and algorithms		
Black Zen software	Carl Zeiss Microscopy GmbH	RRID: SCR_018163
GraphPad Prism 8	GraphPad Software	RRID: SCR_002798
MATLAB	MathWorks Inc.	RRID: SCR_001622
RStudio	RStudio	RRID: SCR_000432
Stereo Investigator	MBF Bioscience, Inc.	RRID: SCR_002526
TopScan system	CleverSys Inc.	RRID: SCR_017141
Other		
Adeno-associated viral vector AAV-CAG-ArchT-GFP (2×10^{11} particles/ml)	UNC Vector Core	N/A